Novel photon-counting low-dose computed tomography using a multi-pixel photon counter

H. Morita[a,*], T. Oshima[a], J. Kataoka[a], M. Arimoto[a], H.Nitta[b]

[a] *Research Institute for Science and Engineering, Waseda University, 3-4-1 Ohkubo, Shinjuku, Tokyo, Japan*
[b] *Hitachi Metals Ltd, Osaka 618-0013, Japan*

Abstract

X-ray computed tomography (CT) is widely used in diagnostic imaging. Owing to a strong radiation exposure associated with this method, numerous proposals have been made for reducing the radiation dose. In addition, conventional CT does not provide information on the energy associated with each X-ray photon because intensity is rather high, typically amounts to 10^{7-9} cps/mm^2. Here, we propose a novel, low-dose photon-counting CT system based on a multi-pixel photon counter (MPPC) and a high-speed scintillator. To demonstrate high signal-to-noise ratio utilizing the internal gain and the fast time response of the MPPC, we compared CT images acquired under the same conditions among a photodiode (PD), an avalanche photodiode and a MPPC. In particular, the images' contrast-to-noise ratio (CNR) acquired using the MPPC improved 12.6-fold compared with the images acquired in conventional CT using a PD. We also performed energy-resolved imaging by adopting 4 energy thresholds of 20, 40, 60, and 80 keV. We confirmed a substantial improvement of the imaging contrast as well as a reduction in the beam hardening for the CT images. We conclude that the proposed MPPC-based detector is likely to be a promising device for use in future CT scanners.

Keywords: Photon counting CT, MPPC, APD, Low dose

*Corresponding author
Email address: hayato-morita@akane.waseda.jp (H. Morita)

1. Introduction

X-ray computed tomography (CT) is a nondestructive technique for visualizing interior organs (e.g., in a human body) by reconstructing many X-ray projection images acquired from different angles. While CT is a key technology in modern medical imaging-based diagnostics, irradiation by high-intensity X-rays is required for acquiring high-resolution and -contrast X-ray images. In some cases, the radiation dose reaches 10 mSv per a CT scan, which is much higher than the average annual radiation dose which a typical adult receives from natural sources, 2.4 mSv [1, 2]. In addition, CT imaging is often conducted several times a year, for follow-up purposes. As a result, CT-delivered radiation is becoming a serious concern for patients.

One commonly used detector in clinical X-ray CT consists of a gadolinium oxysulfide (Gd_2O_2S) scintillator (fluorescent decay time: τ_{GOS} ~3 ms) coupled with a photodiode (PD) that has no internal gain ($M = 1$). Thus, during high-intensity irradiation, such as the one used in CT (typically reaching 10^{7-9} cps/mm^2), all X-rays pile up, so that only a direct current (DC) from the PD can be recorded with sub-second intervals. Thus, conventional CT does not provide information on the energy of individual X-ray pulses. Identifying materials with similar CT values is difficult, which represents a new diagnostic challenge for future CT systems. To address this issue, a photon-counting X-ray CT (PC-CT) system has been developed; this system allows to acquire CT images in different energy bands in a single CT scan. The PC-CT system has been suggested to be advantageous not only for identifying materials but also for alleviating a variety of artifacts (e.g., beam hardening effects) that are specific to X-ray CT [3, 4, 5]. Moreover, the contrast of CT imaging may be enhanced by choosing an optimal energy window for target materials, in which the difference between the materials' absorption coefficients is most pronounced.

Several PC-CT detectors have been proposed up to date. The most commonly studied systems utilize semiconductor devices, e.g., those based on cadmium telluride (CdTe) or cadmium zinc telluride (CZT) [6, 7, 8, 9]. The good

energy resolution of CdTe/CZT devices is advantageous for multi-color imaging, in particular for the so-called "K-edge imaging", which involves two energy bins on both sides of a K-absorption edge. However, mobility of carriers in CdTe/CZT detectors is so slow that the pixel size must be as small as sub-mm to withstand high count rates associated with clinical X-ray CT. Moreover, charge-sensitive amplifiers (CSAs) must be used because CdTe/CZT does not support internal amplification of the signal charge. As a result, the number of read-out channels, including slow-response CSA, is typically very high, making PC-CT systems impractical for clinical use.

In this paper, we characterized a future PC-CT system that uses a multi-pixel photon counter (MPPC) coupled with a high-speed cerium-doped yttrium aluminum perovskite (Ce:YAP) scintillator. The MPPC features silicon photomultipliers (Si-PMs) and is a solid-state photon counting device, consisting of 10^2-10^4 avalanche photodiode (APD) pixels operating in the Geiger mode [10]. Owing to its high avalanche gain ($M \simeq 10^5-10^6$) and fast time response ($\sim$10 ns/pulse), a high signal-to-noise ratio (SNR) can be achieved even for weak light signals with high incident rates. Moreover, the use of CSA is not required; a PC-CT system based on the MPPC and fast scintillator is expected to be rather simple. The major motivation for this study was to evaluate possible advantages associated by using MPPCs in CT imaging, particularly toward future applications to PC-CT scanners with low-dose. To evaluate the effect of the internal gain of different photo-detectors, we first compared an APD and a MPPC with the dimensions of $1\times1\,\mathrm{mm}^2$ for CT imaging, under the same operational conditions as those used for a photodiode (PD) that mimicked a conventional CT system in the current mode operation. Next, we characterized the PC-CT system with the MPPC and performed multi-color imaging using information about X-ray energies in the pulse mode. Finally, we demonstrate that energy-resolved CT imaging improves the imaging contrast and alleviates beam hardening artifacts in CT imaging.

2. Experimental setup

A block diagram of the studied X-ray CT system is shown in Fig. 1. This prototypical CT system consisted of an X-ray generator (Toreck, TRIX-150LE), a turntable (Sigma Koki, SGSP-80YAW), a scan stage (Sigma Koki, OSMS26-200), and an X-ray detection part. The detection part consisted of a pixel scintillator ($1\times1\times1\,\mathrm{mm}^3$) optically coupled with either PD, APD, or MPPC, with the dimensions of $1\times1\,\mathrm{mm}^2$. The distance between the source and the isocenter was 90 cm, and that between the isocenter and the detector was 10 cm. A 1-mm-thick aluminum (Al) filter was placed on the generator's output port to reduce the low-energy X-ray contamination, and a 1-cm-thick copper (Cu) collimator was placed in front of the detector. The turntable and the scan stage were controlled by a personal computer via a two-stage controller (Sigma Koki, SHOT-302GS). CT tomography was performed by repeatedly linearly scanning and rotating the object. In this experiment, the number of projections was 45 per a rotation of 180°. Obtained CT images were reconstructed using the filter back-projection method (FBP) with a ramp filter.

We first acquired CT images using the PD, APD, and MPPC, in the "current" mode readout. Here, the current mode corresponds to the mode in which the average photo-current from the detector is recorded with a certain integration time, as in conventional CT systems. The projection data of objects were acquired by reading out the photo-current values using a source measure unit (Keithley, Model 237) and a personal computer. The exposure time was 0.5 s per pixel. The scintillator was Gd_2O_2S (Hitachi Metals, Ltd), which is widely used in conventional CT systems. We used a photo-sensor S8664-11 (Hamamatsu Photonics) that can be made to function both as a PD ($M = 1$) and an APD ($M = 50$) simply by changing the bias voltage. We used a MPPC of the same size (Hamamatsu Photonics, S12571-010C), operating at $M = 1.35\times10^5$.

In the pulse mode, the number of X-ray pulses is counted by setting multiple energy thresholds, thus enabling to acquire multi-color X-ray images. To withstand as high a count rate as possible, we used a single-crystal Ce:YAP

scintillator, characterized by a fast decay time, τ_{YAP} ~25 ns. The density of Ce:YAP in the scintillator was 5.35 g/cm^3 [11], and the scintillator dimensions were 1×1×1 mm^3, the same as for Gd_2O_2S. The output pulses from the MPPC (S12571-050C) were first amplified using a current-voltage amplifier, and then discriminated by a multi-comparator with 4 energy thresholds of 20, 40, 60, and 80 keV, respectively. Then, a counter card (Contec, CNT3204MT) recorded the number of input X-ray pulses every 0.5 s. We monitored variations in the pulse counts during CT scans, to reconstruct the projection data of phantoms.

3. Comparison of CT images (PD, APD and MPPC)

We used a 6-cm-diameter cylindrical acrylic phantom, filled with water (1.0 g/cm^3). In it, this phantom contained a smaller 2-cm-diameter cylinder, filled with alcohol (0.78 g/cm^3), as shown in Fig. 2. The phantom was scanned using an X-ray tube voltage of 120 kV and a tube current of 0.2 mA. The resulting CT images obtained using the PD, APD, and MPPC in the current mode are shown in Fig. 3. Obviously, the images obtained using the APD (Fig. 3(b)) and MPPC (Fig. 3(c)) are of higher qualities than that obtained using the PD (Fig. 3(a)), such that water and alcohol are clearly discriminated. Especially using the MPPC in the pulse mode, the noise fluctuation is substantially reduced for the acquired image, compared with the image acquired in the current mode, as shown in Fig. 3(d).

We quantitatively analyzed the CT images that were acquired using the PD, APD, and MPPC, by varying the tube current from 0.1 mA to 1.0 mA. In these experiments, the tube voltage was fixed at 120 kV. Fig. 4 shows the variation in the radiation dose at the isocenter, measured using a dosimeter (TOYO MEDIC, RAMTEC-1500). The radiation dose increases proportionally to the tube current. For example, the radiation dose of 4.8 mGy/min was measured for the tube voltage of 120 kV and tube current of 0.2 mA. We evaluated the contrast-to-noise ratios (CNRs) for water and alcohol. The CNR was defined as

$$CNR = \frac{|\mu_M - \mu_B|}{\sigma_B}, \tag{1}$$

where μ_M and μ_B are the linear attenuation coefficients of the target material and background, respectively, and σ_B is the background standard deviation. The region of interest (ROI) was defined as in Fig. 5. ROI_M and ROI_B were the regions of the target material (alcohol) and the background (water), respectively.

Table 1: The CNR and the contrast ratio values of water and alcohol, calculated from all of the CT images in Fig. 3.

	PD	APD	MPPC (current)	MPPC (pulse)
CNR	1.42 ± 1.27	4.41 ± 1.34	5.32 ± 1.40	17.89 ± 1.47
Contrast ratio (μ_M/μ_B)	0.71 ± 0.21	0.70 ± 0.08	0.69 ± 0.07	0.65 ± 0.02

Table 1 lists the CNR and the contrast ratio ($= \mu_M/\mu_B$) values of water and alcohol, calculated from all of the CT images in Fig. 3; these images were acquired with 0.2 mA and 120 kV. The CNR values for the CT images acquired using the APD, MPPC (current), and MPPC (pulse) were 3.1, 3.7, and 12.6 times higher than that for the CT image acquired using the PD, and the contrast ratio was enhanced using the APD and MPPC. Fig. 6 shows the variations in the CNR as a function of the tube current, for the tube current in the 0.1−1.0 mA range. By increasing the tube current, the CNR improves because the image noise is reduced. High CNRs can be obtained by utilizing the APD and MPPC compared with that obtained using the PD, owing to internal amplification. Especially, the CNR value obtained using the MPPC in the pulse mode is much higher than other values, even for small tube current values (i.e., low radiation dose).

4. Multi-colored imaging

Not only a substantial improvement in the CNR is obtained, as described above, but multi-color imaging becomes possible in the pulse mode of the MPPC. Fig. 7(a) shows the X-ray energy spectra obtained using the MPPC

and YAP irradiated at the tube voltage of 120 kV, without setting any energy threshold. A spectral peak at 26.3 keV is visible, while a noisy spectrum is obtained for energies under 10 keV. Fig. 7(b) shows the same spectrum but with the energy threshold of $E_{\rm th} = 20$ keV, and it is of note that the noise under 10 keV is substantially weaker. As photon energy increases, the bremsstrahlung intensity substantially decreased. However, the maximum energy corresponds to the tube voltage of 120 kV. Fig. 8 shows the spectra for the energy thresholds of $E_{\rm th} = 40$, 60, and 80 keV.

As an application of energy-resolved imaging, we first examined how the image contrasts can be enhanced by choosing an appropriate energy window for materials in a phantom. In this context, the linear attenuation coefficients of water (1.0 g/cm^3) and alcohol (0.78 g/cm^3) are shown in Fig. 9. The difference between the linear attenuation coefficients of the materials at lower energies becomes more pronounced. Therefore, water and alcohol are likely to be easier discriminated at lower energies. To test this, the cylindrical acryl phantom that contained water and alcohol was scanned at the tube voltage of 120 kV with the tube current of 0.4 mA (Fig. 10). The energy ranges were 20−40 keV, 40−60 keV, 60−80 keV, and 80−120 keV, and CT images using all X-ray energies were reconstructed and compared with those obtained using conventional CT. The CNR and the contrast ratios of water and alcohol calculated for all of these CT images are listed in Table 2. Clearly, the contrast ratio of alcohol and water are most enhanced in the 20−40 keV range, as shown in Fig. 10. In fact, the contrast ratio calculated using X-rays in the entire energy range (i.e., 20−120 keV) was 0.63, whereas that calculated for the 20−40 keV range was 0.56.

As a second example of multi-color imaging, we examined the alleviation of beam hardening artifacts by utilizing the energy information. It is known that the beam hardening effect yields dark streaks between two high-attenuation objects such as born or metal [13, 14, 15]. To mimic this situation, we prepared another 6-cm-diameter phantom, in which two cylindrical 2-cm-diameter Al objects were included, as shown in Fig. 11. This phantom was scanned at the tube

Table 2: The CNR and the contrast ratio of water and alcohol calculated from each CT image of Fig. 10.

	All energy (20−120 keV)	20−40 keV	40−60 keV	60−80 keV	80−120 keV
CNR	21.34 ± 1.56	18.99 ± 1.43	10.20 ± 1.45	5.74 ± 1.30	2.35 ± 1.31
Contrast ratio (μ_M/μ_B)	0.63 ± 0.02	0.56 ± 0.03	0.67 ± 0.04	0.73 ± 0.05	0.73 ± 0.13

voltage of 150 kV (Fig. 12). The energy ranges were 30−60 keV, 60−90 keV, 90−120 keV, and 120−150 keV. For comparison purposes, we also acquired CT images using the entire range of X-ray energies (30−150 keV), to mimic conventional CT imaging. As shown in Fig. 12, in general beam hardening was strong between the two Al cylinders as seen in the CT images. However, beam hardening was substantially alleviated for higher-energy bands (e.g., 90−120 keV). As a result, most artifacts could be eliminated using energies above 90 keV, but the noise would increase owing to the limited image reconstruction statistics, especially for energies above 120 keV.

5. Discussion and conclusion

5.1. Interpretation of results

In this paper, we evaluated CT images that were acquired using a PD, APD, and MPPC, under the same experimental conditions. The CT images acquired using a conventional PD required high-intensity X-rays for reducing noise and obtaining clear images. In contrast, using either the APD or MPPC and lower radiation dose we obtained images that were clearer than those obtained using the PD. This is because the contribution of the dark current (dark noise) in the photo-sensor was reduced remarkably by the internal amplification of the APD and MPPC. Therefore, the SNR of an image acquired using the MPPC is expected to be much higher than that of an image acquired using the APD,

corresponding to different internal multiplication gains, M=10^5−10^6 (MPPC) and M= 50 (APD).

However, the CNR values for the APD and MPPC in the current mode were almost the same, as shown in Fig. 6. This result suggests that there are other factors contributing to the additional persistent fluctuation in the case of the MPPC. When the MPPC was irradiated with high-intensity X-ray beams, the output DC from the MPPC was above ∼mA, likely increasing the detector temperature. Because the MPPC gain is sensitive to the detector temperature, fluctuations in the avalanche gain will be induced, adding noise to the resultant CT images. Thus, a higher CNR can be obtained if using an appropriate temperature compensation device for the MPPC.

The CNR of the image acquired using the MPPC in the pulse mode was much higher than others, because the noise below the energy threshold was reduced by reading out pulse signals, as shown in Fig. 7. Therefore, the pulse readout from the MPPC enables the acquisition of low-noise CT images, in spite of a low radiation dose. Even for the low tube current of 0.1 mA, which the above-mentioned heating is less significant, the CNR improved more than 10-fold, compared with conventional CT.

Information on the X-rays energy can be also obtained by reading out using the MPPC in the pulse mode. For this, the X-ray pulse energies were divided into 4 energy bins. We showed that by choosing an appropriate energy window, the image contrast is improved and the beam hardening effect is alleviated, as shown in Fig. 10 and Fig. 12. However, we also note that the CT images become noisy owing to poor statistics, resulting in the lower CNR values, as listed in Table 2. Thus, in the future analysis, we will use all of the events rather than events in a specific energy bin, but appropriate weighting will be necessary.

5.2. Comparison with other approaches

There are numerous other proposals to reduce the radiation dose of the CT system. For example, Toshiba Medical Systems have proposed the Adaptive

Iterative Dose Reduction 3D (AIDR 3D) that not only reduces the image noise, but also improves the spatial resolution. By adopting an active collimation technique and tube modulation system optimized for a given anatomical region, AIDR 3D is expected to reduce the dose by up to 40% [16]. Together with newly developed Quantum Denoising Software (QDS), doses in a clinical setting can be reduced by more than 75%. Similarly, GE Healthcare as developed a new method of image reconstruction, Adaptive Statistical Iterative Reconstruction (ASiR), which may provide excellent image quality, even at doses of less than 1 mSv [17]. However, we believe that our proposed system, based on an MPPC, is of great merit, as a 12.6-fold improvement of the CNR suggests a reduction of the radiation dose by more than two orders of magnitude without using any specific image reconstruction algorithm, when implemented in the future CT system.

We also confirm that a PC-CT system based on an MPPC and a high-speed scintillator can produce a superior CNR to those operated in the current mode. This indicates that other detectors, particularly CdTe/CZT, can also produce similar excellent images when operated in a PC-CT mode, although they do not exhibit an internal amplification of signal charge. However, as briefly noted in the introduction section, the slow response of CdTe/CZT detectors requires unnecessarily small sub-millimeter pixel sizes to withstand a high count rate, thus the number of read-out channels becomes huge. While the excellent energy resolution of semiconductor devices seems to be beneficial for K-edge imaging, the energy window must be large enough to not be affected by photon statistics, typically being 10 keV below and above the K-edge, which is easily attainable, even with scintillation detectors. Therefore, we argue that a CT system based on MPPC coupled with a fast scintillator has a vast potential to be used in future PC-CT systems, particularly for low-dose and multi-color imaging. We are, however, in the initial phase of detector development. As a next step, we are developing an MPPC-based CT module, consisting of 4×4 arrays of MPPC and Ce:YAP scintillators directly coupled with a dedicated 16-channel ASIC [18]. The performance of this system will be analyzed elsewhere.

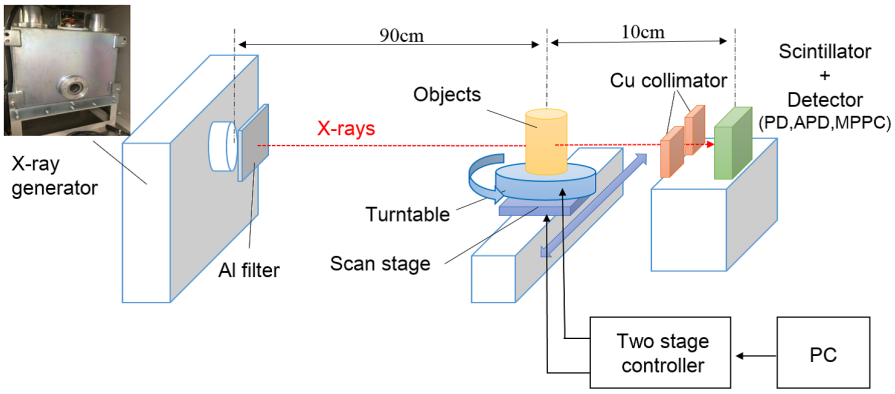

Figure 1: A block diagram of the X-ray CT system described in this paper.

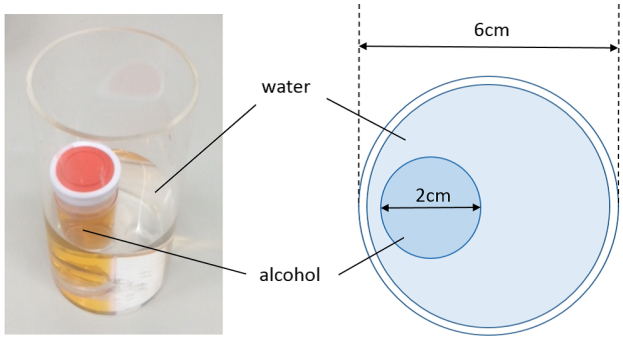

Figure 2: A cylindrical 6-cm-diameter acrylic phantom, filled with water ($1.0\,\mathrm{g/cm^3}$). The phantom included another, 2-cm-diameter, cylinder inside it, filled with alcohol ($0.78\,\mathrm{g/cm^3}$).

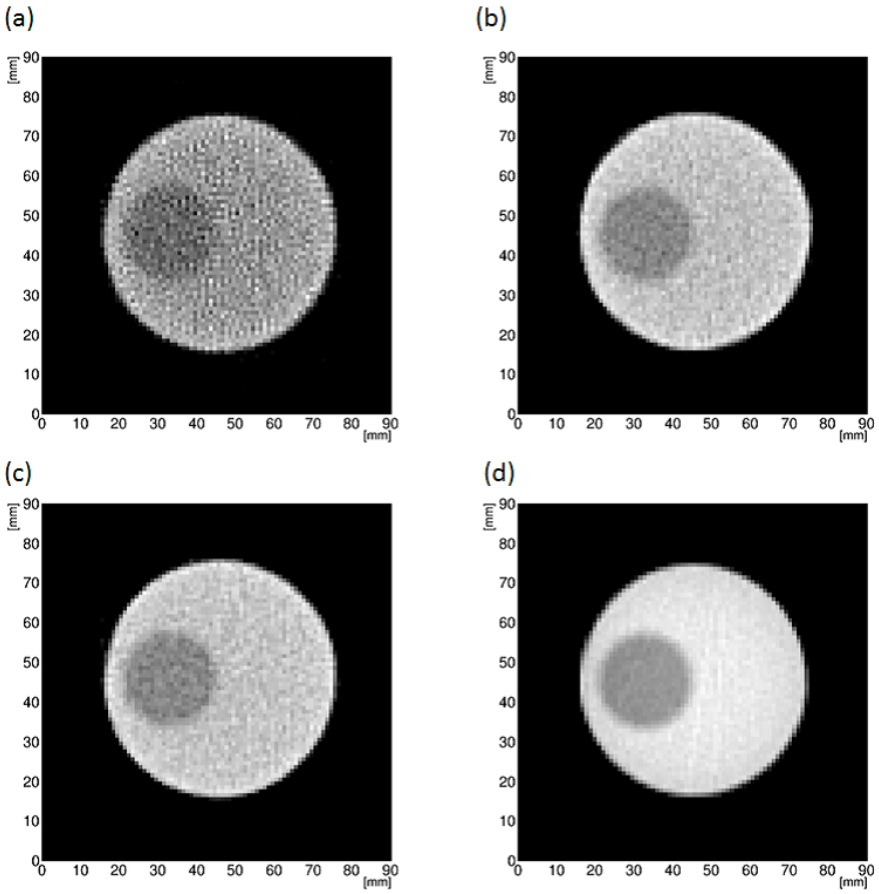

Figure 3: CT images taken for the X-ray tube voltage of 120 kV and the tube current of 0.2 mA for (a) PD, (b) APD, (c) MPPC [current], (d) MPPC [pulse], respectively.

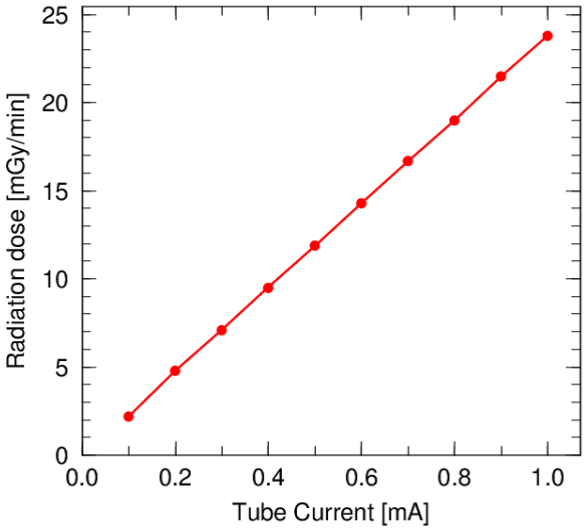

Figure 4: The radiation dose at the isocenter, measured for the tube voltage of 120 kV.

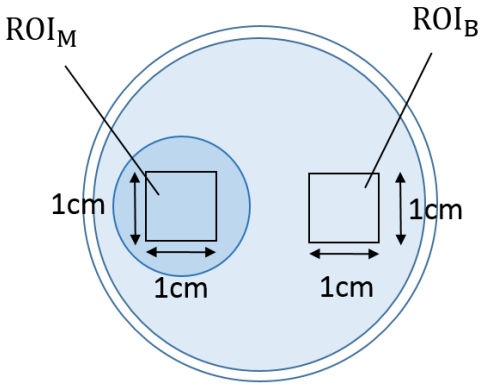

Figure 5: The interest regions of the target material (alcohol), and background (water).

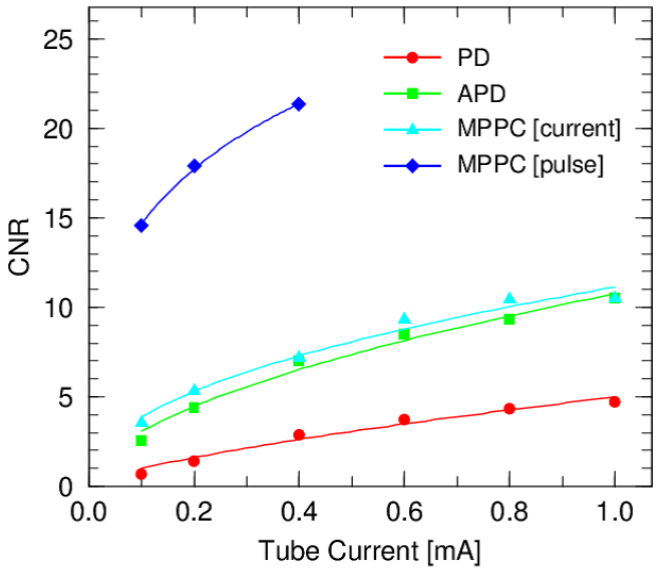

Figure 6: The CNRs of all CT images acquired for the tube current in the 0.1−1.0 mA range.

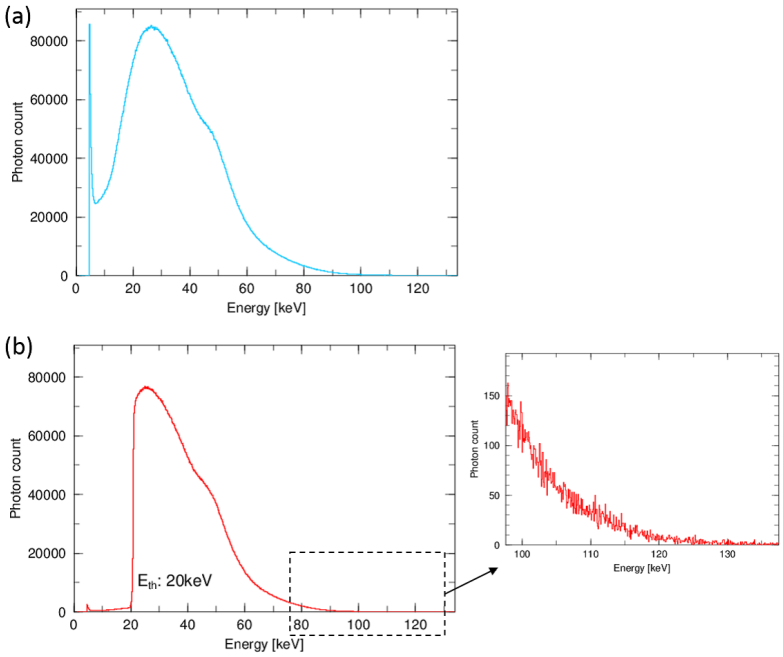

Figure 7: X-ray energy spectra observed using the MPPC and YAP for the tube voltage of 120 kV: (a) without an energy threshold, (b) with the energy threshold of 20 keV. The bremsstrahlung intensity substantially decreased with increasing photon energy, but the maximum energy corresponds to the tube voltage of 120 kV.

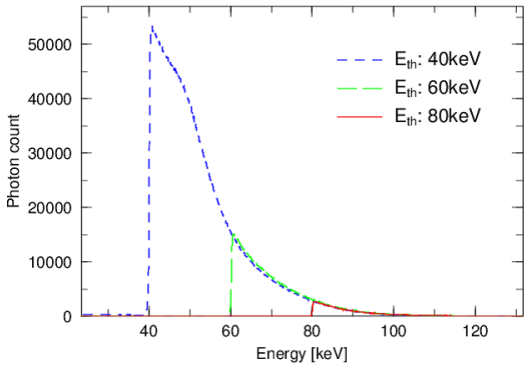

Figure 8: X-ray energy spectra observed using the MPPC and YAP for the tube voltage of 120 kV, with the energy thresholds of 40, 60, and 80 keV, respectively.

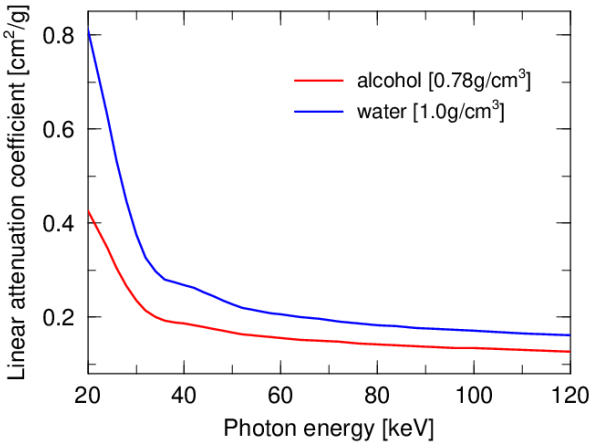

Figure 9: The linear attenuation coefficients of water ($1.0\,\mathrm{g/cm^3}$) and alcohol ($0.78\,\mathrm{g/cm^3}$) [12]

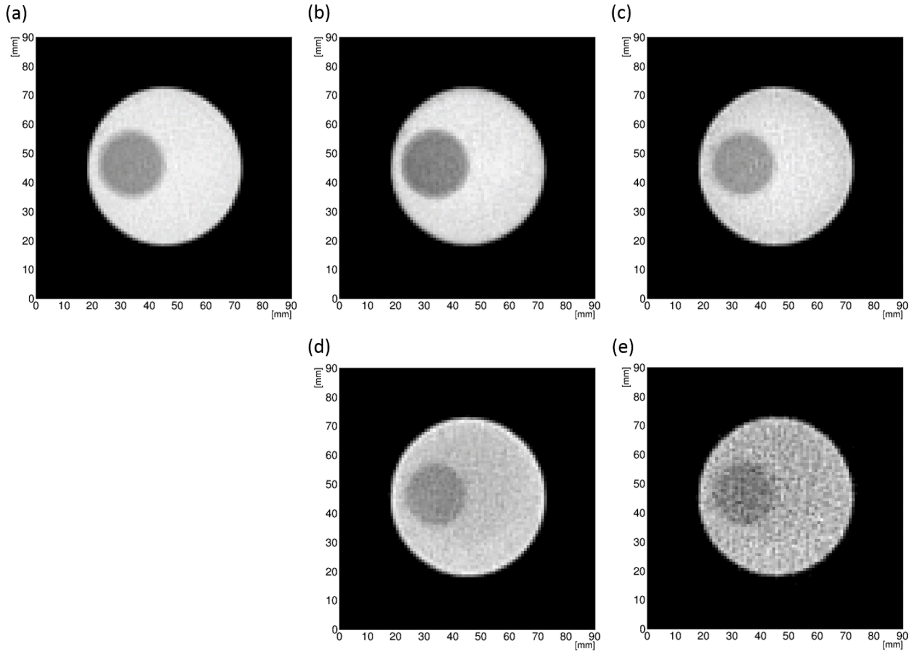

Figure 10: The energy-resolved CT images of a phantom with (a) all energies considered, (b) energy in the $20-40\,\mathrm{keV}$ range, (c) energy in the $40-60\,\mathrm{keV}$ range, (d) energy in the $60-80\,\mathrm{keV}$ range, and (e) energy in the $80-120\,\mathrm{keV}$ range.

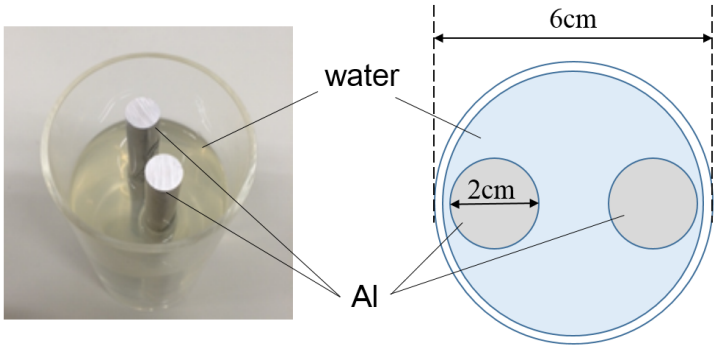

Figure 11: The 6-cm-diameter CT phantom, in which included two cylindrical 2-cm-dameter Al objects were incorporated.

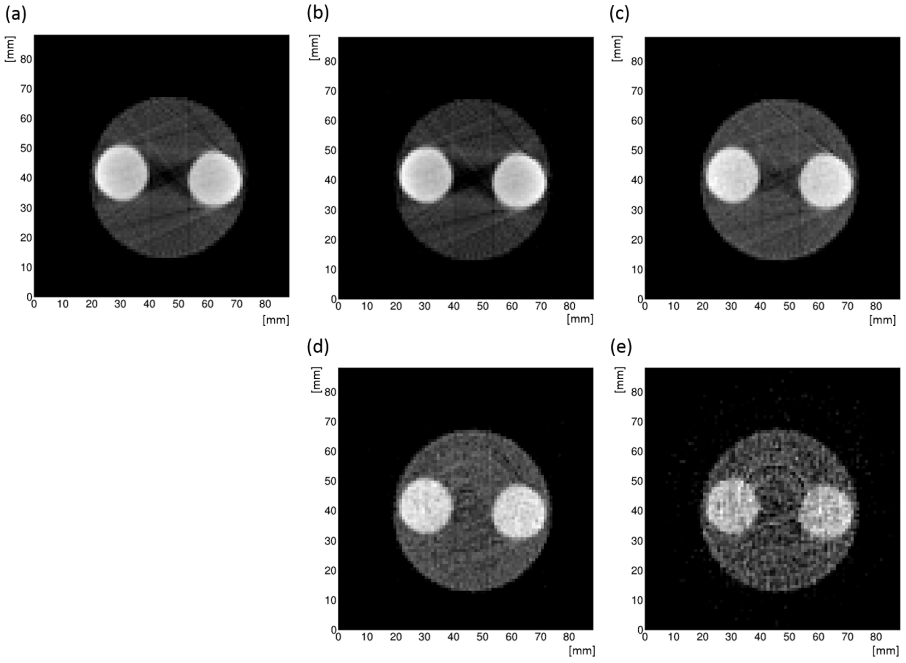

Figure 12: The energy-resolved CT images of the phantom with (a) all energies considered, (b) energy in the 30−60 keV range, (c) energy in the 60−90 keV range, (d) energy in the 90−120 keV range, and (e) energy in the 120−150 keV range.

References

[1] W. A. Kalender, Physics in Medicine and Biology 59 (2014) R129.

[2] J. H. Hendry, et al., Journal of Radiological Protection 29 (2009) A29.

[3] Y. Lee, et al., Nuclear Instruments and Methods in Physics Research A 815 (2016) 68.

[4] H. Kodama, et al., Japanese Journal of Applied Physics 52 (2013) 072202.

[5] E. Sato, et al., Applied Radiation and Isotopes 70 (2012) 336.

[6] K. Ogawa, et al., Nuclear Instruments and Methods in Physics Research A 664 (2012) 29.

[7] Y. Lee, et al., Nuclear Instruments and Methods in Physics Research A 794 (2015) 54.

[8] P. M. Shikhaliev, et al,. Physics in Medicine and Biology 56 (2011) 1905.

[9] H. Matsukiyo, et al., Japanese Journal of Applied Physics 49 (2010) 027001.

[10] J. Kataoka, et al., Nuclear Instruments and Methods in Physics Research A 784 (2015) 248.

[11] P. Lecoq, Nuclear Instruments and Methods in Physics Research A 809 (2016) 130.

[12] National Institute of Standards and Technology, XCOM: Photon Cross Section Database,⟨ http://www.nist.gov/pml/data/xcom⟩.

[13] P. M. Shikhaliev, Physics in Medicine and Biology 50 (2005) 5813.

[14] M. G. Bisogni, et al., Nuclear Instruments and Methods in Physics Research A 581 (2007) 94.

[15] H. S. Park, et al., IEEE Transaction on Medical Imaging, vol.35, No.2, February 2016.

[16] R. Irwan, et al., AIDR 3D - Reduces Dose and Simultaneously Improves Image Quality, https://www.toshiba-medical.eu/eu/wp-content/uploads/sites/2/2014/10/AIDR-3D-white-paper1.pdf, Published 2014, Accessed January 31, 2017.

[17] GE Healthcare, Publications with ASiR, https://www.sarh.es/files/IVJornadaSARH/GE_abstracts_ASiR.pdf, Published 2011, Accessed January 31, 2017.

[18] T. Oshima, et al., Nuclear Instruments and Methods in Physics Research A 803 (2015) 8.